

FINITE ELEMENT ANALYSIS OF DOUBLE-BOLT SHEAR-OUT FRACTURE FAILURE

Adewole Kazeem KAYODE^{1,*}, Leopold MBEREYAHU¹

¹ Department of Civil, Environmental and Geomatics Engineering, University of Rwanda, Rwanda.
* corresponding author: kkadewole@yahoo.com.

Abstract

This paper presents the finite element (FE) analysis of double-bolt shear-out (DBSO) fracture failure. The DBSO fracture shape consists of two oppositely: inclined outer main shear fractures, inner main shear fracture, outer shear lips, and curved inner curved fractures. The DBSO begins with two outer main shear fracture initiations under shear, vertical compressive bending, and sideways bending deformations/stresses followed by the two inner main shear fracture initiations under shear and vertical compressive bending deformations. The outer shear lips occurred under vertical compression bending, shear, and sideways tensile bending stresses/deformations while the two inner curved fractures occur under rotational deformation.

Keywords:

Curved fracture;
Double-bolt shear connection;
Failure analysis;
Shear lips;
Main shear fracture.

1 Introduction

The fracture of connections in steel-frame buildings during the Northridge and Kobe earthquakes [1] and the fracture of the gusset plates of the Minneapolis, Minnesota I-35W bridge deck truss [2] have established the need to consider fracture failure in steel structures. Consequently, there is a need for an understanding of the fracture behavior and failure analysis of connections in steel structures. The end shear-out fracture, which involves the shear tearing out of the steel materials between the two shear planes, one on each side of each bolthole is one of the common fracture/failure modes exhibited by shear connections [3, 4]. Consequently, there is a need for an understanding of the end shear-out fracture/failure behavior and failure analysis.

Fracture failure analysis involves various steps. These steps include visual observation, macroscopic and microscopic fractographic analyses, stress analysis, fracture mode identification, and simulated-service testing [5]. Visual observation reveals the stress and deformation types (tensile, compressive, bending, torsional, or a combination of these stress types) experienced by the fractured members or components. The macroscopic fractographic analysis is conducted to reveal the fracture origin, fracture propagation, and fracture sequence. Microfractographic analysis reveals the fracture mode (ductile or brittle) [1].

Stress analysis is conducted to determine the magnitude and the types of stresses (static or dynamic, axial, shear, torsional or bending, and compressive or tensile) that cause fracture [5]. Analytical, closed-form "machine design and structural" formulas are employed to conduct stress analysis. However, where excessive loading is suspected, using machine design and structural formulas for direct calculation of stresses predict incorrect stress levels, and experimental stress analysis is employed to predict component/member stresses [5]. For components or members with very complex shapes, finite-element (FE) analysis is employed to predict the stress type(s) and the magnitude of the stresses causing failure. FE analysis is also employed to determine the critical locations for strain-gage attachment during experimental stress analysis [5].

The published FE works on the prediction of the shear connection double-bolt shear-out failure (DBSO) e.g. ([4, 6-13] amongst others) focused mainly on predicting only the DBSO ultimate load/capacity without predicting the actual/visible DBSO fracture needed for DBSO fracture failure analysis. The successful simulation of DBSO failure in all the aforementioned published FE works was based on the FE prediction of the maximum stress and or strain along the two shear planes of

each bolthole. Thus, to date, the prediction of the DBSO fracture behavior (fracture initiation and propagation, fracture sequence, fracture mode, and fracture shape) and DBSO fracture failure analysis have not been published.

This paper presents the finite element (FE) analysis of the double-bolt shear-out (DBSO) fracture failure covering the predictions and analyses of the DBSO fracture process or sequence, fracture mode, and fracture shape using the phenomenological shear fracture model. The FE simulation was conducted with the isotropic elastic-plastic and the phenomenological shear damage and fracture models inbuilt in the Abaqus materials library. The details of the isotropic elastic-plastic and the phenomenological shear damage and fracture models are not presented for brevity. Interested readers are referred to [14] and [15], and the several published works of the first author (see [16-19]) for the details of the isotropic elastic-plastic and the phenomenological shear damage and fracture models.

2 Experimental

2.1 Simulation of the structural steel sheet double-bolt shear connection shear-out fracture process

FE simulation was conducted on twelve 10 mm thick double-bolt steel sheet shear connection configurations bolted with 24 mm diameter bolts in 26 mm bolthole diameter that exhibited the shear-out fracture mode in the experimental work of [20] shown in Fig. 1(a). The twelve connection configurations consist of a set of six connection configurations made from the Q550D steel grade and another set of six connection configurations made from the Q690D steel grade. The typical geometrical properties (end distance e_1 , edge distance e_2 , pitch, p_2 , and bolthole diameter d_0 , length L , and width W) of the connections are presented in Fig. 1(b). The connection configuration designations and geometrical properties of the twelve connection configurations considered are presented in Table 1. The models of the connection are shown in Fig. 1(c).

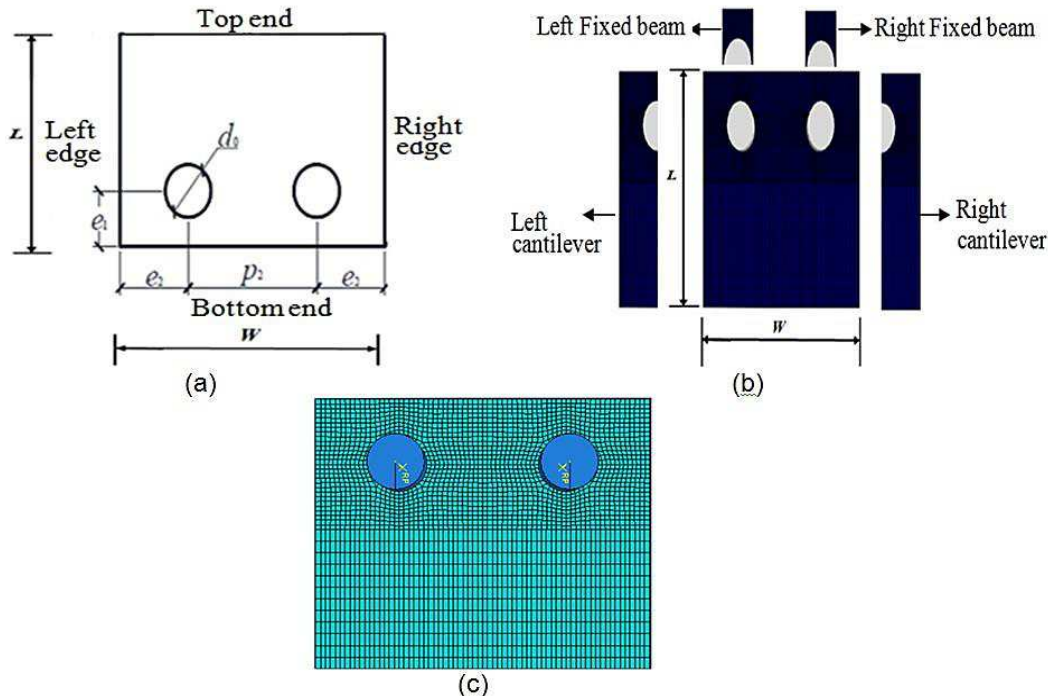


Fig. 1: Double-bolt connection: (a) Configuration and geometric parameters; (b) FE model; (c) FE model of two-bolt connection.

The model of the connections was meshed with 1 mm x 1 mm x 1 mm and 0.5 mm x 0.5 mm x 1 mm C3D8R element sizes downstream and upstream of the boltholes, respectively. The C3D8R element is an 8-node hexahedral linear brick reduced integration element with hourglass control. The combination of the 1 mm x 1 mm x 1 mm element size downstream of the boltholes and the 0.5 mm x 0.5 mm x 1 mm element size upstream of the boltholes represents the optimum mesh sizes

combination that accurately predicted the tensile properties, the shear-out fracture mode and shear-out fracture shape of the connections considered. This optimum mesh size combination was obtained through a mesh convergence study.

The bolts were modeled as a 3D analytical rigid body. The elastic-plastic behavior of the connections made from the Q550D and Q690D steel grades was modeled with the yield strengths of 677 N/mm² and 825 N/mm², tensile strengths of 757 N/mm² and 859 N/mm² and Young moduli of 205GPa and 203GPa respectively obtained from the experimental work of [20]. The simulation of the connections made from the two steel grades was conducted with a density of 7800 kg/m³, and a poisson ratio of 0.3. The fracture simulation was conducted with the calibrated phenomenological shear damage and fracture model parameters for the Q550D and Q690D steel grades obtained from the published work coauthored by the first author (see [21]) which were obtained through the phenomenological curve fitting process. The details of the phenomenological curve fitting process, which involved the FE tensile testing of the Q550D and Q690D steel grades tension coupons validated with the tension test results in the experimental work of [20] are not presented in this work for brevity. The details of the phenomenological curve fitting process are available in the several published works co-authored by the first author (see [16-18]).

Table 1: Connection geometrical properties.

| Steel grade | Connection configuration designation | End distance (mm) | Edge distance (mm) | Pitch (mm) |
|-------------|--------------------------------------|-------------------|--------------------|------------|
| 550 | TH-12-15-24-550 | 12 | 15 | 24 |
| 550 | TH-12-15-27-550 | 12 | 15 | 27 |
| 550 | TH-12-15-30-550 | 12 | 15 | 30 |
| 550 | TH-15-20-30-550 | 15 | 20 | 30 |
| 550 | TH-15-20-35-550 | 15 | 20 | 35 |
| 550 | TH-15-20-40-550 | 15 | 20 | 40 |
| 690 | TH-12-15-24-690 | 12 | 15 | 24 |
| 690 | TH-12-15-27-690 | 12 | 15 | 27 |
| 690 | TH-12-15-30-690 | 12 | 15 | 30 |
| 690 | TH-15-20-30-690 | 15 | 20 | 30 |
| 690 | TH-15-20-35-690 | 15 | 20 | 35 |
| 690 | TH-15-20-40-690 | 15 | 20 | 40 |

The general contact (explicit) algorithm with the tangential behaviour, penalty frictional interaction, and a coefficient of friction of 0.15 (a value between the 0.0 and 0.3 employed in the published literature) were employed to model the contact between the steel sheet models and the bolts. The simulation of the connection fracture test was conducted by pulling the bottom end of the model of the connection that is free to move only in the vertical longitudinal/tensile loading direction downwardly against the fixed bolts.

3 Results

The FE simulations conducted on the twelve connection configurations presented in Table 1 made from the Q550D and Q690D steel grades predicted accurate force-displacement curves and predicted the same DBSO deformation-to-fracture sequence and fracture shape. For brevity, only the predicted and experimental force-displacement curves for two out the six connection configurations made from the Q550D and the Q690D steel grades covered by the FE simulation conducted in this work are presented in Fig. 2. Also, for brevity, only the typical DBSO deformation-to-fracture sequence and fracture shape are presented in Figs 3 to 10.

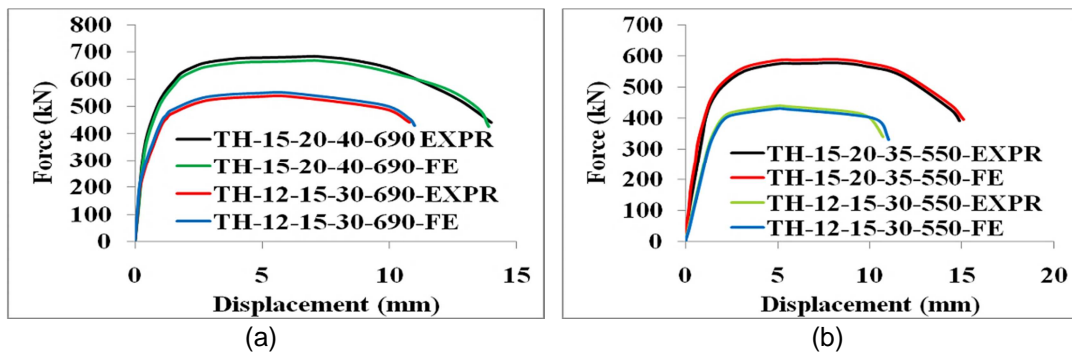


Fig. 2: Force-displacement curves: (a) Connections made from Q690D steel grades; (b) Connections made from Q550D steel grades.

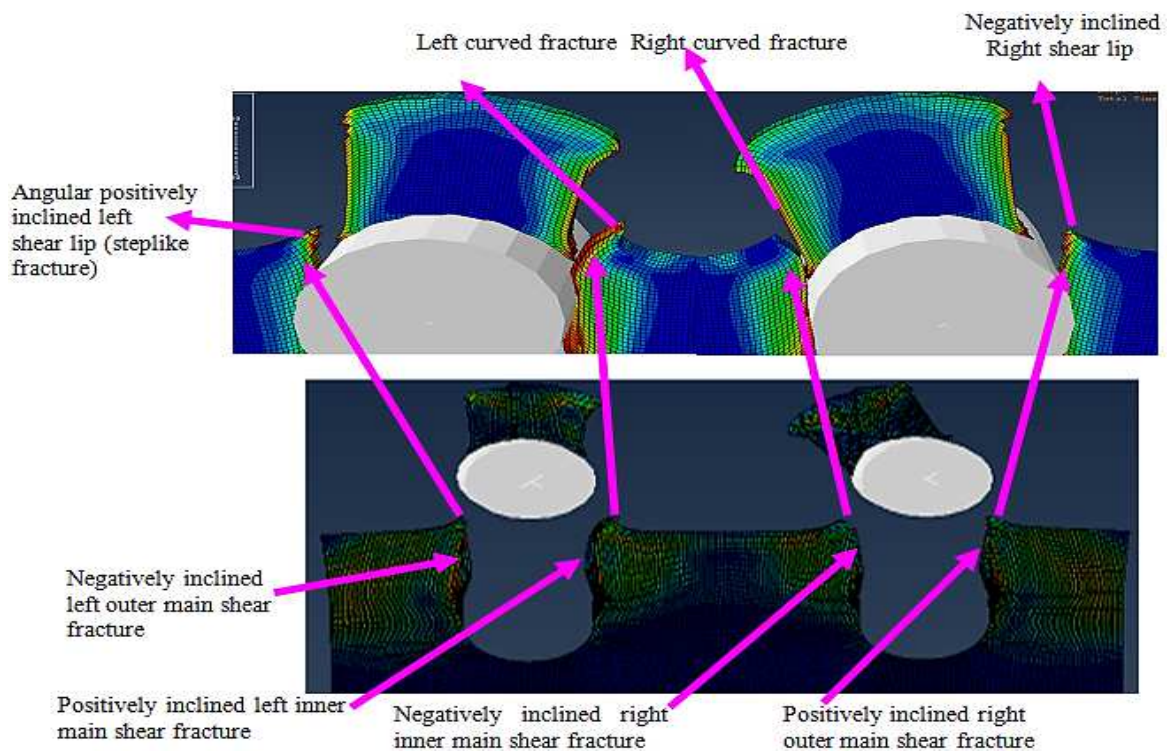
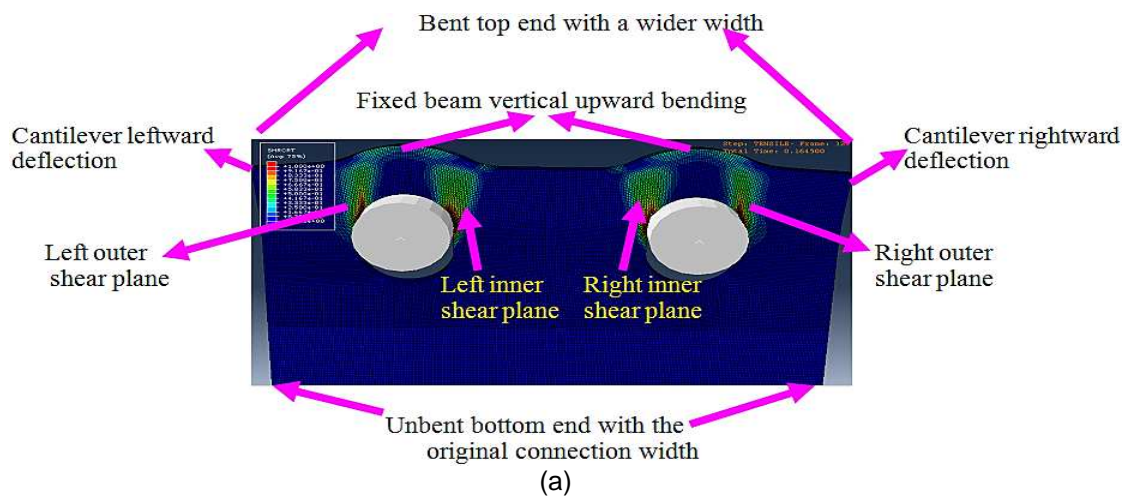
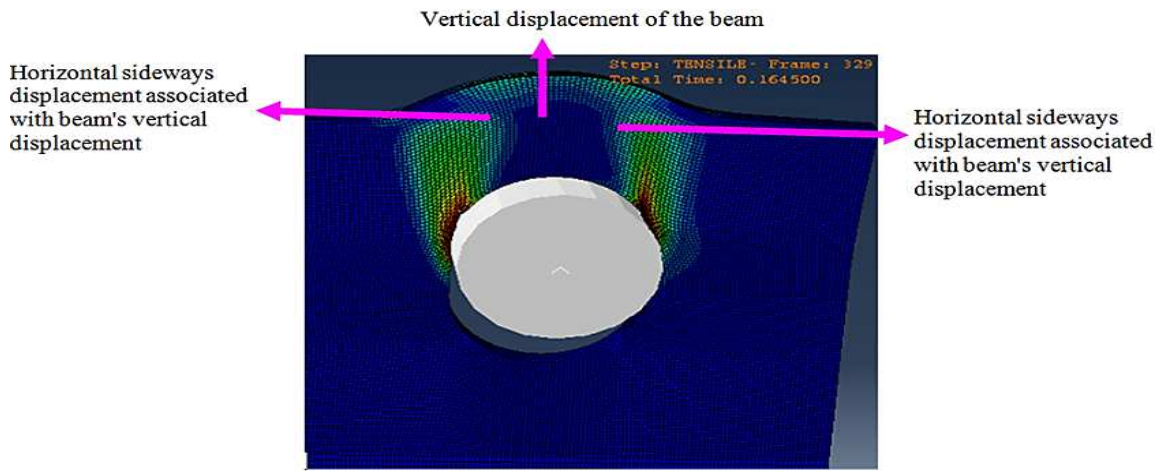


Fig. 3: Predicted steel sheet connection DBO fracture shape.





(b)

Fig. 4: DBSO failure mode deformed shape at the ultimate load and up to prior to fracture initiation: (a) Fixed beam vertical displacement and bending, and cantilever sideways bending; (b) Horizontal sideways displacement associated with beam's vertical displacement.

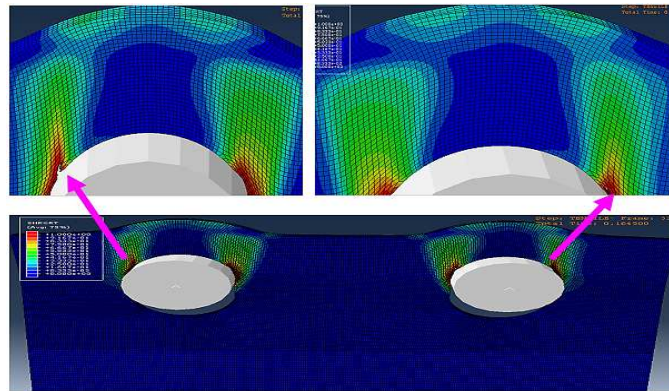


Fig. 5: First stage of the steel sheet connection DBSO fracture process.

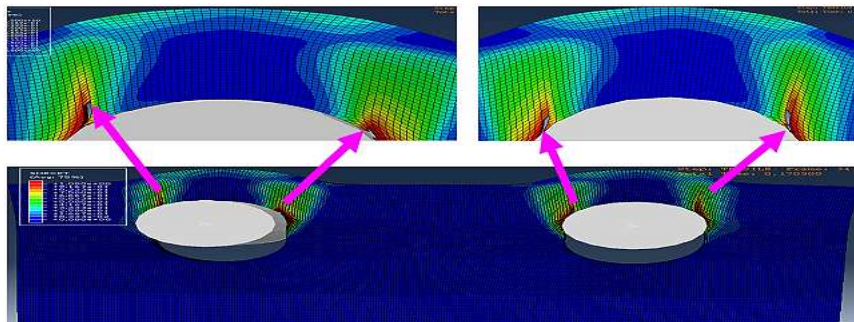


Fig. 6: Second stage of the steel sheet connection DBSO fracture process.

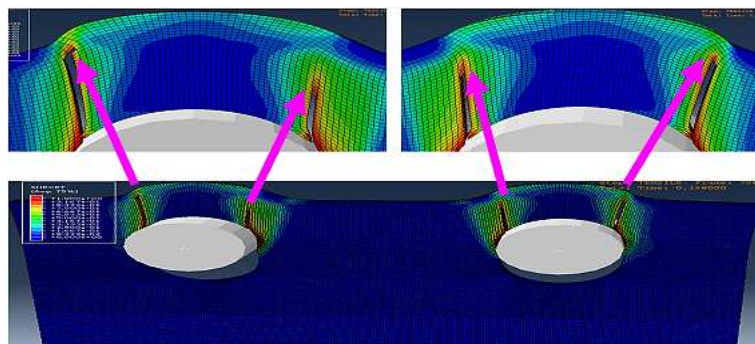


Fig. 7: Third stage of the steel sheet connection DBSO fracture process.

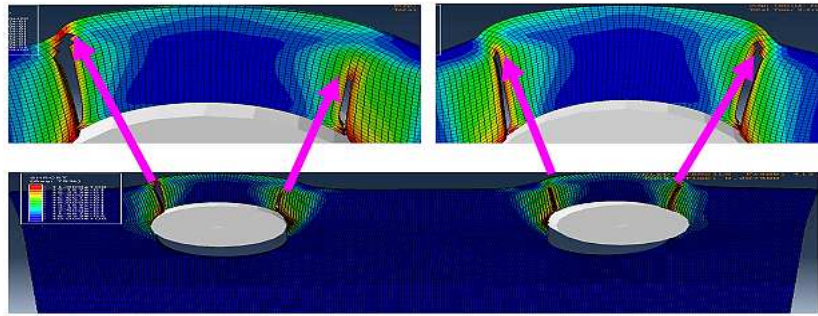


Fig. 8: Forth stage of the steel sheet connection DBSO fracture process.

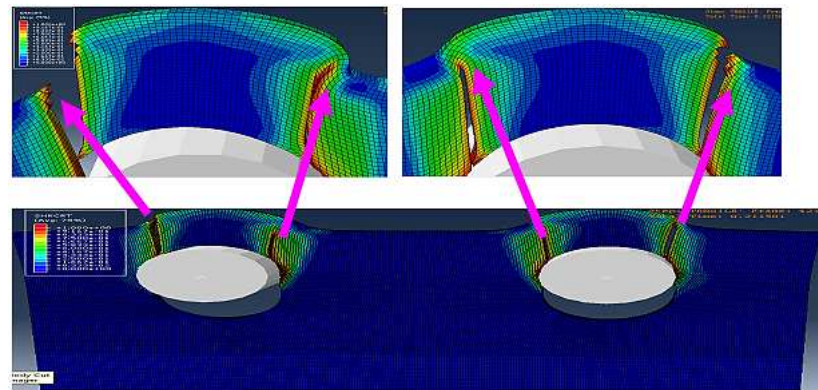


Fig. 9: Fifth stage of the steel sheet connection DBSO fracture process.

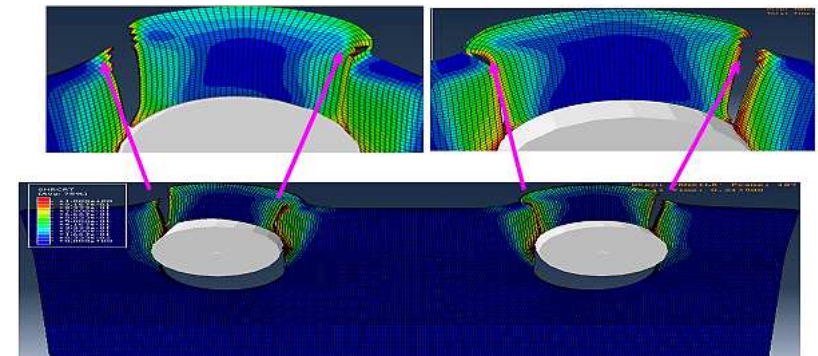


Fig. 10: Sixth stage of steel sheet connection DBSO fracture process.

4 Discussions

4.1 Accuracy of the predicted DBSO tensile properties and fracture mode

As shown in Fig. 2, the good agreement between the experimental work of [20] and the predicted force-displacement curves demonstrates the accuracy of the FE in predicting the tensile response of the four double-bolt connection configurations made from the Q690D and Q550D steel grades. As shown in Fig. 3, the typical fracture mode predicted for all the connections with the designations and geometric parameters shown in Table 1, which exhibits a fracture mode with the steel sheet between the inner and the outer shear planes of both boltholes torn out represents the end shear-out fracture mode. This result demonstrates the accuracy of the FE in predicting the shear-out fracture mode exhibited by the two-bolt connections in the experimental work of [20].

4.2 Accuracy of the predicted DBSO fracture shape

As shown in Fig. 3, the predicted DBSO fracture shape consists of four fracture surfaces. Two (left and right) outer fracture surfaces, each with a long inclined shear fracture which begins from the outer shear plane of each bolthole surface and ends with the short angularly inclined shear fracture (shown by the steplike fracture propagation) from the end of the outer long shear fracture to the end of the connection. Two inner fracture surfaces, each with a long inclined shear fracture which begins

from each bolthole surface inner shear plane and ends with a curved fracture from the end of the inner long shear fracture to the end of the connection. The long and the short inclined shear fractures are referred to as the main shear fracture and the shear lip (shown by the steplike fracture), respectively. The main shear fracture on one side of each bolthole is oppositely inclined to the main shear fracture on the other side (i.e., the inner and the outer main shear fractures of each bolthole are oppositely inclined).

Fractures that resulted from the rightward propagation, such as the left inner main shear fracture, the right outer main shear fracture (Fig. 5 to 7), and the left shear lip (Fig. 7 to 9), are positively inclined. Fractures that resulted from the leftward propagation, such as the left outer main shear fracture, the right inner main shear fracture (Fig. 5 to 7), and the right shear lip (Fig. 7 to 9), are negatively inclined. The left and right curved fractures formed through rightward and leftward fracture propagations, respectively (Fig. 9 and 10), are taken as positive and negative curves, respectively.

As shown in Fig. 3, the shear lips are oppositely inclined to the outer main shear fracture. Thus, the left outer main shear fracture is negatively inclined, while the left shear lip is positively inclined. Similarly, the right outer main shear fracture is positively inclined, while the right shear lip is negatively inclined. Unlike the shear lips that are oppositely inclined to the outer main shear fractures, the curved fractures have the same fracture propagation orientation as the main inner shear fractures. Thus, both the left inner main shear fracture and the left curved fracture exhibit the same rightward (positive) fracture propagation, while both the right inner main shear fracture and the right curved fracture exhibit the same leftward (negative) fracture propagation. The predicted DBSO fracture shape analysed/described in the preceding sentences agrees well with the DBSO fracture shape in the experimental work of [20], which demonstrates the accuracy of the FE simulation in predicting the DBSO fracture shape.

4.3 Analysis of the deformed shape of the connections that exhibited the DBSO failure mode at the ultimate load and before fracture initiation

The predicted deformed shape of the connections at the ultimate load and before fracture initiation (Fig. 4) with a wider top width and the two arch-shaped bulged-out portions agrees well with the deformed shape at the ultimate load exhibited by the two-bolt connections that exhibited the DBSO failure in the experimental works of [4, 6, 20]. This result demonstrates the accuracy of the FE in predicting the deformed shape of double-bolt connections that exhibit the shear-out failure at the ultimate load and before fracture initiation.

4.4 Analysis of the deformation leading to the DBSO failure mode top wider width at ultimate load

Wang et al. [20] observed that the "rotation of net cross-section" (i.e., the rotation of the material between the left bolthole and the left edge of the connection, and the rotation of the material between the right bolthole and the right edge of the connection) occurred in all the connections that exhibited the shear-out fracture mode. Thus, based on the deformation analysis by [20], the wider top edge/width can be attributed to the leftward rotation of the material between the left bolthole and the left edge of the connection, and the rightward rotation of the material between the right bolthole and the right edge of the connection about the net cross-section of the connections. However, as shown in the predicted deformed shape in Fig. 4 and in the experimental deformed shape of the double-bolt shear connections presented by [4, 6, 20], the widening of the connection from the top end extended beyond the location of the net cross-section and continued up to the bottom of the connection. Consequently, the widening of the connection is not due to the rotation of the material between the bolthole and the edges of the connection about the net cross-section alone. It is due to the leftward bending of the material between the left bolthole and the left edge of the connection, and the rightward bending of the material between the right bolthole and the right edge of the connection across the entire length, L (edges) of the connection.

The material between the left bolthole and the left edge of the connection and the material between the right bolthole and the right edge of the connection across the entire length (free edges) of the connection behaves like a cantilever, which bends leftward and rightward respectively about the bottom end of the connection and are referred to as the left and right cantilevers (Fig. 1b) respectively. The cantilever is bent at its top end, which is at the top end of the connections by the outward (leftward and rightward) horizontal displacements accompanying/associated with the vertical upward displacement of the material in the bulged-out section as shown in Fig. 4b. The largest

deflection of the cantilever occurred at the end of the cantilever, which is at the top end of the connections, resulting in the largest widening at the top of the connection.

4.5 Analysis of the deformation leading to the DBSO failure mode arch-shaped bulged-out portions at the ultimate load

The left and right arch-shaped bulged-out portions resulted from the upward deflection of the steel sheet upstream of the boltholes, which behave like beams and are referred to as the left and right fixed beams. The fixed beams have a span equal to the bolthole diameter and a semicircular lower surface profile. The fixed beams are subjected to push-bending by pulling them against the stationary bolts. Thus, the arch-shaped bulged-out sections are bent left and right fixed beams. The arch-shaped bulged-out sections (bent left and right fixed beams) experienced the following three types of deformation due to their upward deflection:

- a) a high shear stress/strain/deformation close to the end of the span of the fixed beam between the net and the gross shear areas/lengths,
- b) a combined tensile and bending (tensile bending) stress/strain/deformation at the crown/peak of the bulged-out section,
- c) a combined compressive and bending (compressive bending) stress/strain/deformation at its bolthole surface.

4.6 DBSO fracture failure process

The first stage of the DBSO fracture process involved the simultaneous left and right outer main shear fracture initiations at the outer shear planes of the left and right bolthole surfaces without any fracture initiation at the two inner shear planes as shown in Fig. 5. Fracture initiation began only at the left and right outer shear planes without any fracture initiation at the inner shear planes because the outer shear planes are subjected to three types of stresses/deformations while the inner shear planes are subjected to only two types of stresses/deformations. The three types of deformation/stress at the outer shear planes are the shear deformation/stress and the compressive bending deformation/stress on the bolthole surface due to the upward bending of the fixed beam, and the tensile bending deformation due to the sideways (leftward and rightward) bending of the cantilever. The two types of deformation at the inner shear planes are the shear deformation/stress and the compressive bending deformation/stress on the bolthole surface due to the upward bending of the fixed beam. The inner shear planes are not subjected to the tensile bending deformation due to the sideways (leftward and rightward) bending because unlike the free edges that are free to deform sideways, the steel plate material between the two inner shear planes is not free to deform sideways. Thus, the resultant stress/deformation at the two outer shear planes due to the combined effects of the three types of deformations/stresses is more than the resultant stress/deformation at the two inner shear planes due to the combined effects of the two types of deformations/stresses leading to the fracture initiation at the two outer shear planes.

The second stage of the DBSO fracture process involved the simultaneous leftward and rightward propagations of the left and right outer main shear fractures, respectively, and the simultaneous left and right inner main shear fracture initiations at the inner shear planes of the two boltholes as shown in Fig. 6. The third stage of the DBSO fracture process involved the continued propagations of the inner and outer main shear fractures, as shown in Fig. 7. At this stage, the two outer main shear fractures are conspicuously longer than the two inner main shear fractures, have propagated completely, and transited to the left and right shear lips as shown by the shear lip fracture initiations at the outer sections of the left and right bulged-out portions in Fig. 7. The fourth stage of the DBSO fracture process involved the rightward and leftward propagations of the initiated left and right shear lips and the continued propagation of the two inner main shear fractures as, shown in Fig. 8. The fifth stage of the DBSO fracture process involved the complete propagation of the left and right shear lips leading to the complete fracture of the two outer shear planes and the continued propagation of the two inner main shear fractures as shown in Fig. 9.

The sixth stage of the DBSO fracture process involved the anticlockwise and clockwise rotations of the partially fractured/torn-out portion of the left and right fixed beams about the remaining ligament on the left and right inner shear planes respectively, leading to the left and right curved fracture initiations (Fig. 10). The partially fractured/torn-out portions of the left and right fixed beams were subjected to twisting/rotation because the material along the outer shear planes that held them in position and ensured that they hitherto underwent vertical upward deflection from the

first to the sixth fracture process stages had fractured. The last stage of the DBSO fracture process involved the complete rightward and leftward propagations of the left and right curved fractures leading to the completely fractured connection with curved fractures at the end of the inner shear planes as shown in Fig. 3.

4.7 Analysis of the deformation leading to the DBSO fracture shape

As shown in Fig. 9, the two outer and inner main shear fractures, and the two outer shear lips are inclined and not parallel to the vertical tensile loading direction because they occurred under a combined shear, compressive bending and tensile bending deformations/stresses and not under pure shear deformation/stress. Fracture under pure shear deformation/stress is parallel to the vertical tensile loading direction. As shown in Fig. 3, the outer shear lips have an angular inclination to the outer main shear fractures and to the vertical tensile loading direction while the fractures from the tip of the inner main shear fractures to the top end of the connection are curved. This is because the inclined outer shear lips are formed under combined shear, compressive bending, and tensile bending deformations/stresses, while the curved fractures are formed under rotational deformation/stress only.

5 Conclusions

The finite element (FE) analysis of the shear-out fracture failure in double-bolt shear connections is presented. The FE failure analysis covers the deformation-to-DBSO fracture initiation, fracture process/propagation, and fracture shape analyses. The DBSO fracture shape consists of two oppositely inclined outer main shear fractures, two oppositely inclined inner main shear fractures, two oppositely inclined outer shear lips, and two oppositely orientated inner curved fractures. The two outer shear lips are angularly inclined to the outer main shear fractures and to the vertical tensile loading direction throughout the portion of the connection from the tip of the two outer main shear fractures to the end of the connection. Conversely, the two inner curved fractures exhibit curvature throughout the portion of the connection from the tip of the two inner main shear fractures to the end of the connection. The shear lips have an opposite inclination to the outer main shear fractures, while the curved fractures exhibit the same fracture propagation orientation as the inner main shear fractures.

FE analysis reveals the following: The DBSO fracture initiation does not begin simultaneously at the inner and outer shear planes. The DBSO fracture begins with the two outer main shear fracture initiations, followed by the two inner main shear fracture initiations. Fracture initiations begin only at the outer shear planes because the resultant stress/deformation at the two outer shear planes due to the combined effects of three types of deformations/stresses (shear, compressive upward bending, and sideways bending deformations/stresses) is more than the resultant stress/deformation at the two inner shear planes due to the combined effects of only two types of deformations/stresses (shear and compressive upward bending deformations).

The two outer main shear fractures in DBSO propagate faster than the two inner main shear fractures and transit to the two outer shear lips that propagate to the complete fracture of the outer shear planes followed by the transition of the two inner main shear fractures to two curved fractures. The two curved fractures propagate to the complete fracture of the inner shear planes. The outer shear lips occur under a combined upward compression bending, shear, and sideways tensile bending stresses/deformations while the two curved inner fractures occur under rotational deformation alone. This work thus establishes the steel sheet connection DBSO fracture failure sequence/process, and the types of deformations/stresses at the various stages of the steel sheet connection DBSO fracture failure process that are essential for the steel sheet connection DBSO fracture failure analysis.

References

- [1] KANVINDE, A. M. - DEIERLEIN, G. G.: Finite-Element Simulation of Ductile Fracture in Reduced Section Pull-Plates Using Micromechanics-Based Fracture Models. *Journal of Structural Engineering*, 2007, DOI: 10.1061/(ASCE)0733-9445(2007)133:5(656), pp. 1-39.
- [2] PRZYWARA, J. - KAPIL, K.: Failure in Structural Steels and Overview of I-35W, Bridge Collapse. University of Notre Dame, 2017, <https://www3.nd.edu/~cpssl/group/work/Failure-in-Structural-Steels-and-Overview-of-I-35W-Bridge-Collapse.pdf>. Assessed on 24/06/2018.

- [3] ROGERS, C. A. - HANCOCK, G. J.: Failure Modes of Bolted Sheet Steel Connections Loaded in Shear. Research Report No R772, Centre for Advanced Structural Engineering, Department of Civil Engineering, Sydney NSW 2006, AUSTRALIA, <http://www.civil.usyd.edu.au>, assessed 20th May, 2016.
- [4] MOŽE, P. - BEG, D. A complete study of bearing stress in single bolt connections. *Journal of Constructional Steel Research*, 95, 2014, pp. 126–140.
- [5] VANDER VOORT, G. F.: Visual examination and light microscopy, ASM Handbook, Vol. 12, Fractography, ASM International, Materials Park, Ohio, 1987, pp. 91–165.
- [6] MOŽE, P. - BEG, D.: High strength steel tension splices with one or two bolts. *Journal of Constructional Steel Research* 66, 2010, pp. 1000-1010.
- [7] KIM, T. - KUWAMURA, H.: Finite element modelling of bolted connections in thin-walled stainless steel plates under static shear. *Thin-Walled Structures* 45, 2007, pp. 407–421
- [8] KIM, T. - KUWAMURA, H.: Numerical investigation on strength design and curling effect of mechanically fastened joints in cold-formed austenitic stainless steel. *Materials and Design*, 32, 2011, pp. 3942–3956.
- [9] KIM, T. S. - HAN, B. S.: Numerical Simulation and Effect of Curling on Bolted Connections in Cold-formed Stainless Steel. *ISIJ International*, Vol. 47(6), 2007, pp. 920–929.
- [10] KIM, T. S. - KUWAMURA, H. - KIM, S. - LEE, Y. T. - CHO, T.: A parametric study on ultimate strength of single shear bolted connections with curling. *Thin-Walled Structures*, 46, 2008, pp. 38–53.
- [11] KIM, T. S. - KUWAMURA, H. - KIM, S. - LEE, Y. T. - CHO, T.: Investigation on ultimate strength of thin-walled steel single shear bolted connections with two bolts using finite element analysis. *Thin-Walled Structures*, 47, 2009, pp. 1191–1202.
- [12] DRAGANIĆ, H. - DOKŠANOVIĆ, T. - MARKULAK, D.: Investigation of bearing failure in steel single bolt lap connections. *Journal of Constructional Steel Research*, 98, 2014, pp. 59–72.
- [13] SALIH, E. L. - GARDNER, L. - NETHERCOT, D. A.: Bearing failure in stainless steel bolted connection. *Engineering Structures*, 33, 2011, pp. 549–562.
- [14] HOOPUTRA, H. - GESE, H. - DELL, H. - WERNER, H. A.: Comprehensive failure model for crashworthiness simulation of aluminium extrusions. *International Journal of Crashworthiness*, 9(5), 2004, pp. 449–64.
- [15] SIMULIA 2007: Abaqus documentation, Abaqus Incorporated, Dassault Systemes, 2007.
- [16] ADEWOLE, K. K. - BULL, S. J.: Prediction of the fracture performance of defect-free steel bars for civil engineering applications using finite element simulation. *Construction and Building Materials*, 41, 2013, pp. 9 –14.
- [17] ADEWOLE, K. K. - BULL, S. J.: Numerical Prediction of Differences in Micromechanical Fracture Sequence in Notched and Un-Notched Wires for Civil Engineering Applications. *Civil Engineering Dimension*, Vol. 16, No. 2, Sept. 2014, pp. 87-95.
- [18] ADEWOLE, K. K. - TEH, L. H.: Predicting Steel Tensile Responses and Fracture Using the Phenomenological Ductile Shear Fracture Model. *Journal of Materials in Civil engineering*, American Society of Civil Engineers, 2017, 06017019-6, DOI: 10.1061/(ASCE)MT.1943-5533.0002094.
- [19] ADEWOLE, K. K. – OLUTOGE: Numerical prediction of structural steel flat and slant fracture modes using phenomenological shear fracture model. *Journal of King Saud University - Engineering Sciences*, 31, 2017, pp. 234 – 237, DOI: 10.1016/j.jksues.2017.11.001.
- [20] WANG Y. B. - LYU, Y. F. - LI, G. Q.: Experimental investigation of two-bolt connections for high strength steel members. 12th International Conference on Advances in Steel-Concrete Composite Structures (ASCCS 2018). Universitat Politècnica de València, València, Spain, June 27-29, 2018, <http://dx.doi.org/10.4995/ASCCS2018.2018.7211>.
- [21] ADEWOLE, K. K. - ADESOGAN, S. O.: Finite Element Single-Bolt Shear Connection Shear-Out Fracture Failure Analysis. *Journal of Failure Analysis and Prevention*. Vol. 18, Issue 3, 2018, pp. 659 – 666, <https://doi.org/10.1007/s11668-018-0457-x>.